Pearlite Development in Commercial Hadfield Steel by Means of Isothermal Reactions

M. Martín, M. Raposo, O. Prat, M. F. Giordana & J. Malarría

Metallography, Microstructure, and Analysis
Application and Innovation for Metals, Alloys, and Engineered Materials

ISSN 2192-9262

Metallogr. Microstruct. Anal.
DOI 10.1007/s13632-017-0391-4

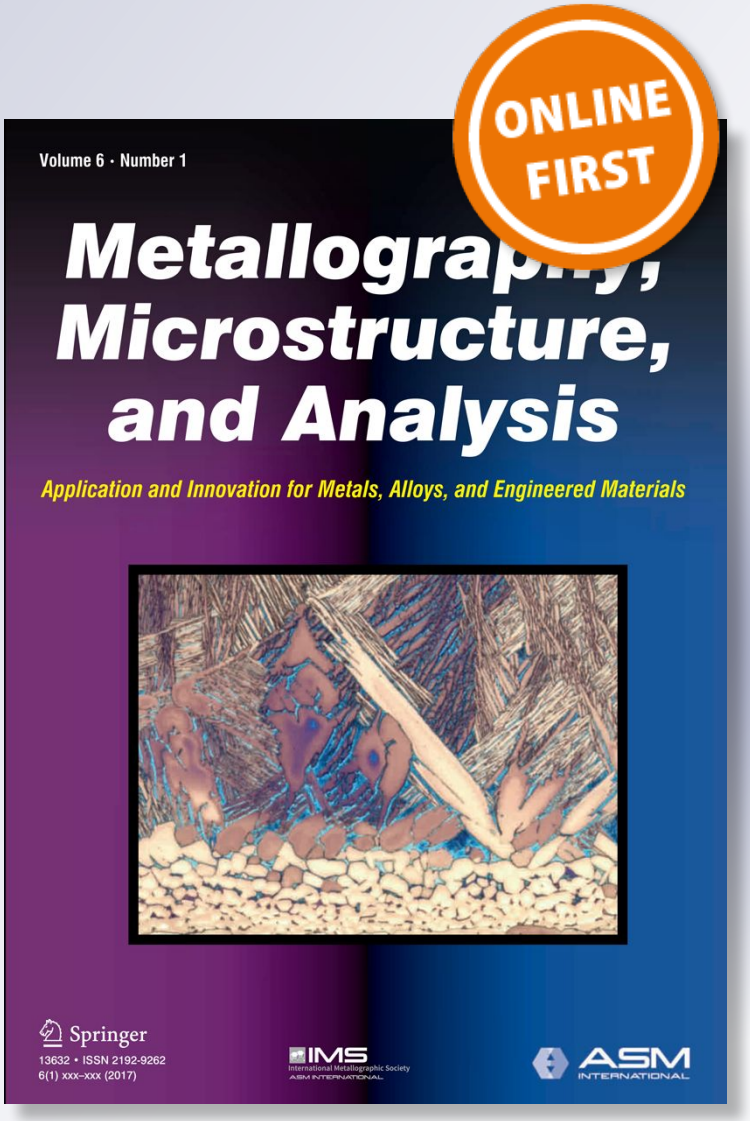

Springer

Metallogr. Microstruct. Anal.
DOI 10.1007/s13632-017-0391-4

TECHNICAL ARTICLE

Pearlite Development in Commercial Hadfield Steel by Means of Isothermal Reactions

M. Martín[1] · M. Raposo[1] · O. Prat[2] · M. F. Giordana[1] · J. Malarría[1]

Received: 20 July 2017 / Revised: 11 September 2017 / Accepted: 21 September 2017

Abstract The Fe–12Mn–1C Hadfield steel is an abrasion-resistant alloy of high technological relevance for mining and heavy machinery. This composition is susceptible to pearlite formation which is detrimental for the material's ductility. Although its spread use, the study of pearlite formation has been preserved to laboratory conditions which cannot be transferred to industrial practices. This manuscript provides updated information about this phenomenon by constructing the time–temperature-transformation diagram of the alloy between 400 and 600 °C. The pearlitic reaction occurs above 450 °C and begins on the grain boundaries. Only 7 min is needed for the transformation to start at 550 °C, and a maximum pearlite fraction of 35% is reached after 150 min at this temperature. Results are compared with the Fe–12Mn–0.8C composition mostly found in literature. The discussion comprises the effects of carbon and manganese content on the pearlitic reaction with the support of thermodynamics calculations.

Keywords Hadfield steel · Isothermal reaction · Pearlite · TTT-diagram · Thermodynamics

Introduction

The Hadfield manganese steel is widely employed by industry at conditions where high abrasion resistance is needed. Despite its commercial relevance, there are few contributions relating microstructure and mechanical properties of Hadfield steel. In a previous work, the authors showed that pearlite formation can occur in commercially produced Fe–12Mn–1C steel and reduce mechanical properties [1]. A presence of 20% of pearlite in the as-received condition was reported and found responsible for a 90% reduction in elongation at fracture [1]. Similarly, the embrittlement of the material has been related to the formation of pearlite in laboratory casts after solution treatment followed by slow cooling [2]. Such detrimental effects motivated a further investigation on the development of pearlite for this material.

The study of pearlite formation in Hadfield steel has been historically linked to the pearlitic reaction itself. This means the analysis of pearlite nucleation, pearlite growth, and the crystallographic relationships between pearlite constituents and the parent phase. Namely, the alloy has played a secondary role by constituting an appropriate model for studying the nature of pearlite. The reason why the Hadfield steel is chosen is due to its high carbon and manganese content which guarantee the stability of the untransformed austenite upon cooling [3–7].

A milestone in this matter was set by Dippenaar and Honeycombe who conducted their investigation with a material of composition Fe–12Mn–0.8C [7]. That contribution has strongly influenced subsequent scientific research on pearlite nucleation up to present days. A proof of that is the establishment of the chemical composition Fe–12Mn–0.8C as a model to investigate the pearlitic reaction. Such is the case of the works of Hackney and

✉ M. Martín
martin@ifir-conicet.gov.ar

[1] Institute of Physics Rosario CONICET-UNR, 27 de Febrero 210 bis, Rosario, Argentina

[2] Materials Engineering Department, Universidad de Concepción, Edmundo Larenas 270, Concepción, Chile

Published online: 05 October 2017

Shiflet [3–6], Zhou and Shiflet [8], Hutchinson and Shiflet [9], and recently Ontman and Shiflet [10]. These investigations deal with isothermal heat treatments which last for hours and days in order to accomplish fundamental investigations. Some examples of long reaction times are 7 h [7], 18 h [3], 120 h [11], 5 days [9] and up to 120 days [10]. Thus, the motivation of answering fundamental questions has overlooked the technological aspects of pearlite formation in Hadfield steel. Consequently, the available information on this phenomenon cannot be transferred to production or processing condition existing at industrial facilities.

The present work deals with the susceptibility of Fe–12Mn–1C Hadfield steel to undergo pearlite formation. It is shown that pearlite formation can actually occur in a relative short time at conditions easily found at steel plants and post-processing operations. The results are compared with the available information on the Fe–12Mn–0.8C steel. The experimental data within this work are of special interest for the heat treatment of large-sized pieces.

Materials and Experimental Procedure

The alloy under investigation is a commercial Hadfield steel of nominal composition Fe–12Mn–1C and a mean grain size of 100 μm, see Table 1. The as-received material possesses a 20% of pearlite, while the solution-annealed condition presents a fully austenitic microstructure after 15 min at 1050 °C followed by water quenching. A detailed characterization of both conditions by means of optical microscopy, x-ray diffraction, secondary electron microscopy and fractography is presented in [1].

Transmission electron microscopy (TEM) was performed in the as-received condition using a FEI CM200UT operated at 200 kV. TEM circular samples of 3 mm in diameter were mechanically grinded to 100 μm in thickness and then electropolished using a double jet TENUPOL 5. A solution of 900 ml ethanol and 100 ml perchloric acid was used as electrolyte at 25 °C and 65 V. The ultimate thinning was performed with a PIPS GATAN 691 ion mill, operated at 5 keV during 5 h.

The phase diagram of the Fe–12Mn–C system was obtained by means of the Thermo-Calc software, and the database TCFe8 was used for the modeling. The composition Fe–12Mn–1C–0.32Si–0.1Cr, see Table 1, was computed for equilibrium calculations, and the phases graphite and M_5C_2 were rejected for mapping calculations.

Isothermal reactions were carried out employing a differential scanning calorimeter Shimadzu DSC-60. Cylindrical specimens of 3 mm in diameter and 4 mm in length were obtained from the annealed material by means of electrical discharge machining. The cylinders were subjected to a heating rate of 50 °C/min, then isothermally held at the reaction temperature, and afterward cooled to room temperature at 100 °C/min by adding liquefied nitrogen into the DSC refrigerant tank. The reaction temperatures varied between 400 and 600 °C with steps of 50 °C and holding times of 15, 30, 90 and 150 min, respectively. The heat-treated samples were conditioned through standard metallographic preparation and etched with a 5% nital solution. Three micrographs were obtained for every condition, and the pearlite fraction was quantified by means of the image processing and analysis software ImageJ. The isothermal reaction curves were derived by means of the Johnson–Mehl relationship expressed by Eq 1 [12] where $f(t)$ is the transformed fraction, N the rate of nucleation, G the growth rate and t the time.

$$f(t) = 1 - e^{-\frac{\pi}{3}NG^3t^4} \quad (1)$$

Table 1 Chemical composition measured by optical emission spectroscopy (wt.%)

Condition	C	Si	Mn	Cr	Fe
As-received	1.01	0.32	12.6	0.1	Bal.
Annealed (15 min–1050 °C)	1.00	0.33	12.7	0.1	Bal.

Results

Exemplary curves of the detrimental effect of pearlite on the ductility of the alloy are depicted in Fig. 1. The as-received microstructure responsible for the severe drop in elongation to rupture is presented in Fig. 2a. The optical

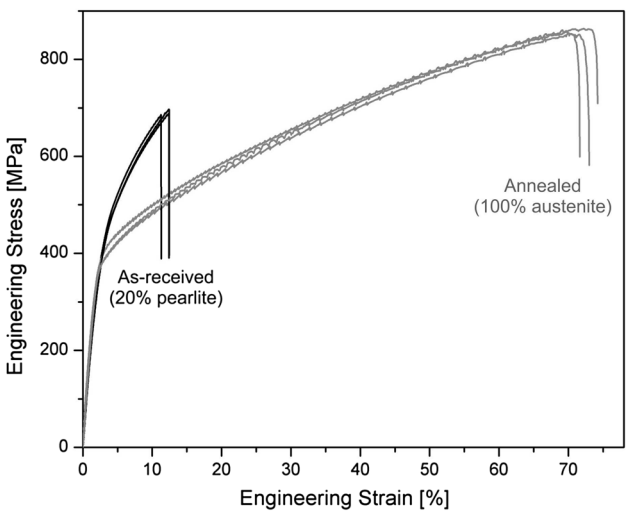

Fig. 1 Engineering stress–strain curves of commercially produced Fe–12Mn–1C Hadfield steel: as-received and solution-annealed conditions

micrograph shows a secondary phase decorating the grain boundaries and forming islands within the grains. High-magnification scanning electron micrographs developed the lamellar microstructure of both type of formations, Fig. 2b. By means of TEM analysis, the presence of extremely thin lamellas was revealed, as shown in Fig. 2c. The lamellar microstructure develops straight and accommodates itself by undergoing branching. A mean value of 30 nm ± 7 nm was obtained for the lamellar spacing.

Figure 2c also presents the electron diffraction pattern of a pearlite colony on the upper-right corner. This pattern is constituted by two different structures: BCC ferrite (α) and complex orthorhombic cementite (θ). Figure 2d shows the key diagram of the diffraction pattern. Circular shape spots were indexed as $[-1\ 1\ 3]_\alpha$ zone axis, while square spots as $[1\ 0\ 0]_\theta$ zone axis [13].

The evaluation of pearlite formation began with the calculation of the phase diagram corresponding to the system Fe–C–12Mn–0.32Si–0.1Cr. Figure 3 presents the result of the thermodynamic equilibrium calculations with a dashed line indicating the 1% carbon isopleth. As pointed out within the figure, the eutectoid composition occurs at a carbon content of 0.34% for this system and 606 °C. With a hypereutectoid composition of 1% carbon, the alloy presents an austenitic one-phase field above 854 °C. By decreasing temperature, a two-phase field of austenite plus cementite develops between 854 and 625 °C. Between 625 and 494 °C, the ferrite phase becomes thermodynamically stable and a three-phase field occurs. Further down, only the ferrite and cementite phases are thermodynamically stable. Computing the phase diagram allowed defining the upper limit of the isothermal heat treatments at 600 °C. The lower limit was set at 400 °C, 94 °C below the transformation line of the three-phase field, to cover a larger temperature range of industrial interest.

Figure 4 shows the microstructures obtained after isothermal treatments varying time and temperature. As can be seen, the transformation begins at the grain boundaries, while the amount of intragranular colonies increases with time. Both growth patterns reach a homogenous distribution after 150 min at 550 and 600 °C, with a pearlite fraction of 35 and 33%, respectively. No transformation was detected at 400 nor at 450 °C within the investigated reaction times. The same happens for the condition 500 °C/15 min where no transformation occurs. A detailed imaging of the initial stages of pearlite formation is represented in Fig. 5. High-magnification SEM micrographs show the incipient formation of pearlite colonies on austenitic grain boundaries after 15 min of isothermal treatment at 550 and 600 °C, respectively. The high-magnification micrographs reveal the presence of intragranular pearlite colonies as well. Table 2 presents the average transformation percentage obtained by means of image analysis in every case.

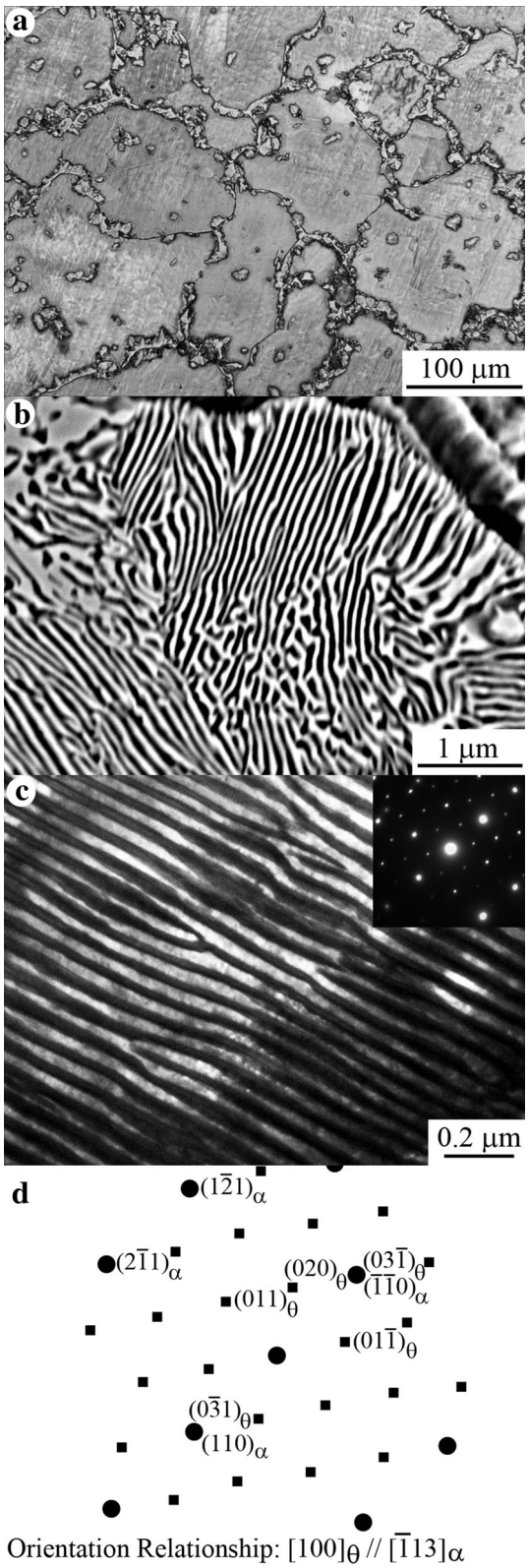

Fig. 2 As-received microstructure of Fe–12Mn–1C Hadfield steel. (**a**) Optical micrograph; (**b**) scanning electron micrograph; (**c**) bright field TEM image of a pearlite colony—the inset shows the corresponding diffraction pattern; (**d**) key diagram of the $[100]_\theta$// $[-113]_\alpha$ diffraction pattern

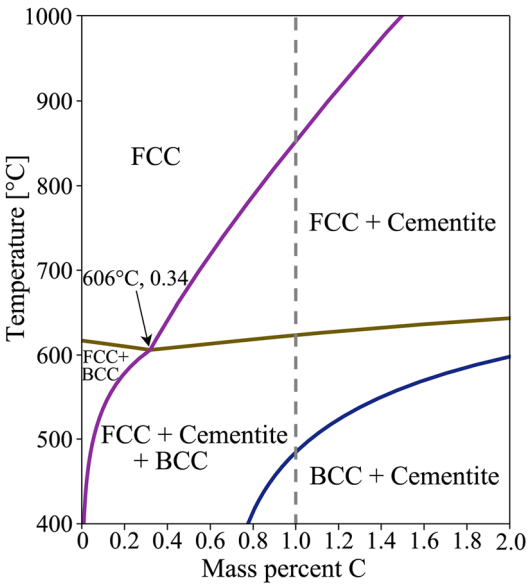

Fig. 3 Calculated phase diagram of the system Fe–12Mn–0.32Si–0.1Cr

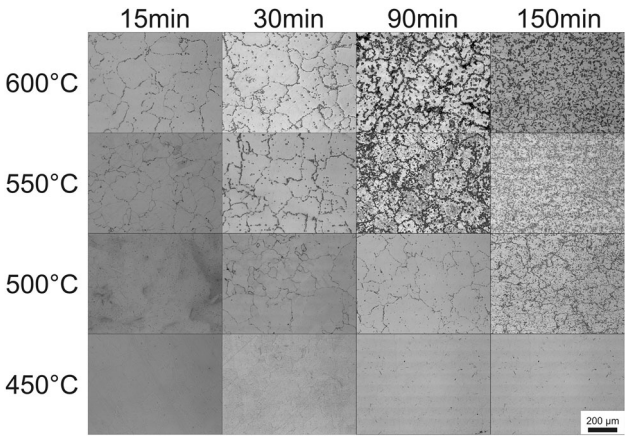

Fig. 4 Microstructures obtained by means of isothermal reactions. The transformation occurs above 450 °C

The experimental data presented in Table 2 were employed to build up the isothermal reactions curves. Sigmoidal functions were obtained for each temperature according to Johnson–Mehl assuming nucleation and growth rate as constants and expressing time in seconds, using Eq 1 [12]. In the following, the time–temperature-transformation diagram was obtained out of the isothermal reactions curves. Figure 6 shows the TTT-diagram of the Fe–12Mn–1C Hadfield steel in solid line and the results of Dippenaar–Honeycombe for a Fe–12Mn–0.8C steel in dashed line [7]. As can be seen, an increase in carbon content from 0.8 to 1% significantly accelerates the pearlitic reaction. While 40 min is needed to start the reaction at 550 °C for 0.8% carbon, 1% dashed curve, a 15% of transformation is obtained at the same time–temperature condition for the Fe–12Mn–1C Hadfield steel. Similar temperatures are obtained for the noses of the 1% curves representing the initiation of the transformation for the Fe–12Mn–1C and the Fe–12Mn–0.8C composition, 564 and 556 °C, respectively. Such temperatures are about 60 °C lower than the one obtained for laboratory casts of Fe–13.3Mn–0.9C–0.2Si composition, which corresponds to an 8-min-long isothermal heat treatment [14]. Table 3 lists the reaction times of the three alloys at 550 °C.

Discussion

Reviewing the literature of pearlite formation in Hadfield steel gives the impression that this phenomenon can only occur under laboratory conditions. Most of the available information refers to very long isothermal treatments to promote pearlite formation. However, the findings in commercially produced Hadfield steel suggest that such long treatments are not mandatory for pearlite to occur [1].

It is known that pearlite formation is preceded by ferrite in the case of hypoeutectoid steels and by cementite in hypereutectoid steels [14–16]. With the hypereutectoid composition of the Hadfield steel, the formation mechanism of pearlite comprises the precipitation of cementite and the formation of ferrite. After a cementite nucleus precipitates, the surrounding austenite is depleted of carbon and the driving force for ferrite formation is increased. Through the formation of a ferrite nucleus adjacent to the cementite, the process repeats itself and the colony can grow stepwise by lateral movements [3, 4, 7, 8, 11]. In order for that to occur, both cementite and ferrite must be thermodynamically stable at the transformation temperature.

As shown in Fig. 4, the pearlitic reaction develops between 500 and 600 °C within the investigated time and temperature interval. In this temperature range, the phases austenite, ferrite and cementite coexist, Fig. 3. Additional information on thermodynamic stability was obtained by computing the amount of the phases in equilibrium as a function of temperature, as shown in Fig. 7. In accordance with Fig. 3, the three phases are stable between 490 and 625 °C, while austenite disappears below 490 °C. At 500 °C, the majority phases are ferrite and cementite with mole fractions close to 0.8 and 0.2, respectively. The prevalence of both phases continues up to 585 °C where the austenite reaches a 0.42 fraction. This means that between 500 and 585 °C there is a high chemical driving force available for the precipitation of ferrite and cementite. In addition to the thermodynamic stability of the phases, the alloying elements are also involved in the formation of pearlite. Particularly, the functions of carbon and manganese are essentials.

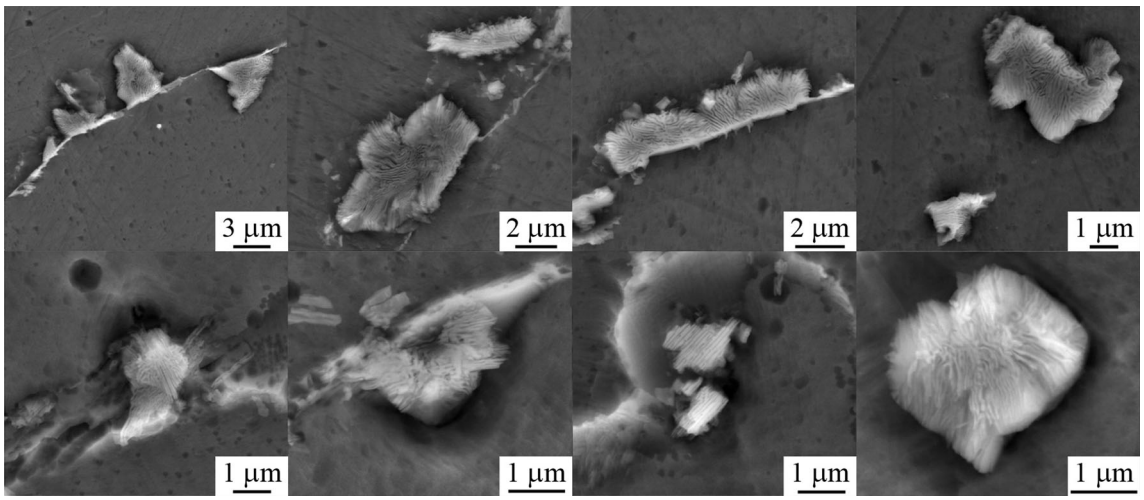

Fig. 5 Development of pearlite colonies after 15 min of isothermal treatment at 600 °C (upper row) and 550 °C (lower row). Right side images correspond to intragranular pearlite colonies

Table 2 Average transformation percentage obtained by image analysis (± 1%)

	15 min	30 min	90 min	150 min
600 °C	3	12	34	33
550 °C	3	9	29	35
500 °C	…	2	5	20
450 °C	…	…	…	…
400 °C	…	…	…	…

(…) No transformation detected

The role of carbon and manganese on pearlite formation in Fe–C–Mn alloys is presented in the literature by means of two mechanisms. Both of them refer to carbon and manganese diffusion. The first mechanism assumes that during pearlite growth all elements are distributed between the cementite and the ferrite phase. Thus, the growth of pearlite occurs under local equilibrium being controlled by manganese which is the element with the lowest diffusion coefficient [17]. The second mechanism considers the temperature range at which the transformation takes place [18]. For low temperatures, the model proposes that pearlite formation is controlled by carbon diffusion neglecting the diffusion of manganese, i.e., the reaction occurs under para-equilibrium mechanism. For higher temperatures, it is considered that manganese diffusion occurs in the interface pearlite–austenite. This is based on the very small diffusion distances at the pearlite–austenite interface and on the higher diffusivity of manganese at the considered temperature. Thus, at lower temperatures the diffusion of carbon is predominant in the formation of pearlite, while at higher temperatures the pearlite growth is controlled by diffusion of manganese through the pearlite–austenite interface. The meaning of "low" and "high" temperatures will depend on the chemical composition of the alloy under study in every case. Particularly, it was mentioned in the Results section that the TTT-nose of the composition Fe–12.6Mn–1C–0.3Si investigated here is located at 564 °C, while for the alloy Fe–13.3Mn–0.9C–0.2Si introduced in [14] it is encountered at 620 °C. It is quite likely that this shifting to higher temperatures is related to a pearlite growth mechanism aided by manganese diffusion [18].

Another feature which has direct relationship with the chemical composition is the amount of single-phase cementite to be present in the microstructure. In the composition Fe–13.3Mn–0.9C–0.2Si presented by Ono et al. [14], the presence of cementite is detected by means of optical microscopy prior to pearlite formation, whereas in this contribution the formation of pearlite is observed at the early stages of isothermal reactions as shown in Fig. 5. This difference in the encountered amount of cementite is attributed to the role of manganese and silicon in the formation of cementite. While manganese stabilizes cementite, silicon inhibits its formation [19, 20]. Concerning manganese, it forms the Mn_3C carbide which is isostructural with cementite allowing both phases to create a solid solution over the whole compositional range $Fe_{3-x}Mn_xC$ [21]. Thus, manganese stabilizes and lowers the temperature at which the cementite starts to precipitate [19, 20]. On the other hand, the incorporation of silicon in steels is generally related to its capability on delaying and inhibiting the formation of cementite during isothermal treatments [19, 20]. The final effect will depend on the added amount of silicon, which is recommended to be at least 0.3 wt.% to reduce the kinetic of cementite formation [20]. The slower progress of the reaction is accompanied by an increase in the temperature

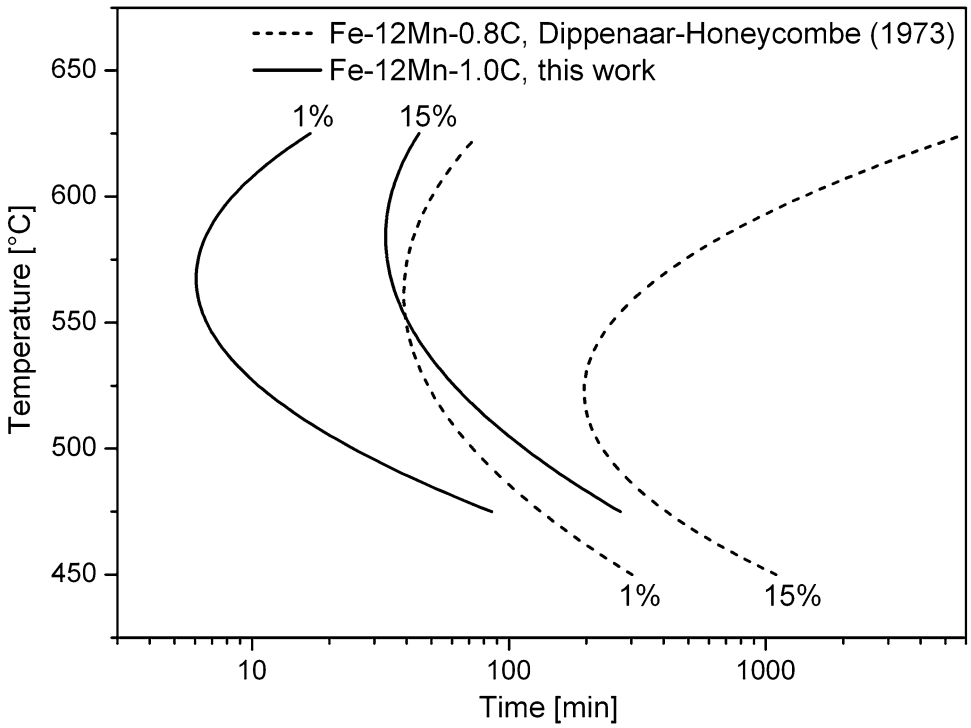

Fig. 6 Time–temperature transformation for commercial Fe–12Mn–1C Hadfield steel and Fe–12Mn–0.8C steel [7]

Table 3 Comparison of transformation times at 550 °C in minutes (min)

Pearlite fraction	Fe–12Mn–0.8C, [7]	Fe–12Mn–1C, this work	Fe–13Mn–0.9C, [14]
1%	40	7	17
15%	250	41	…

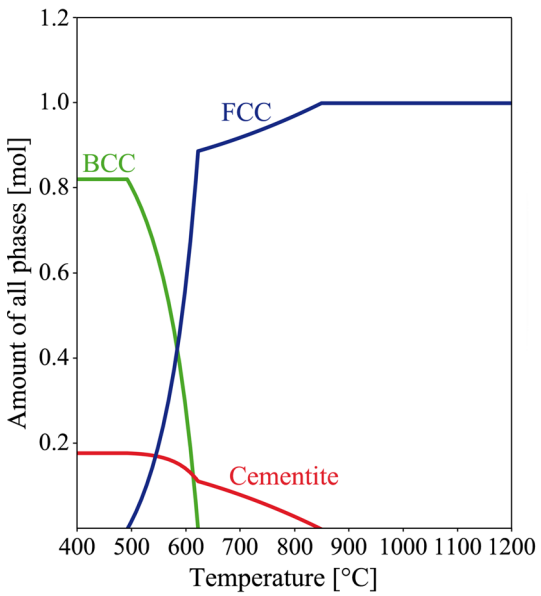

Fig. 7 Calculation of amount of phases versus temperature. With FCC = austenite, BCC = ferrite and cementite

at which cementite starts to precipitate [20]. Opposite to manganese, silicon has an extremely low solubility in cementite. This leads to a silicon concentration buildup at the front of the cementite embryo which is detrimental for its growth [19]. Therefore, the observation of single-phase cementite presented in [14] responds to a combination of higher manganese and lower silicon which simultaneously favors cementite formation. Consistently, the Fe–12.6Mn–1C–0.3Si composition studied in here seems to delay cementite formation allowing an earlier formation of pearlite.

The influence of carbon on the reaction kinetics is clearly observed in Fig. 6 where the development of pearlite in the Fe–12Mn–1C alloy is much more accelerated in comparison with the Fe–12Mn–0.8C composition. This effect can be interpreted out of the phase diagram presented in Fig. 3. As long as the carbon content increases from the eutectoid composition, 0.34%, the A_{cm} line goes up and the austenite becomes less stable with respect to cementite precipitation. This results in a shorter incubation time for the precipitation of cementite and consequently the transformation to pearlite becomes faster [22].

As already mentioned, manganese is involved in pearlite formation by undergoing partitioning and contributing to pearlite growth [10, 23, 24]. The last is indicated to occur at "high" temperatures, which in this case was evaluated by computing the concentration of

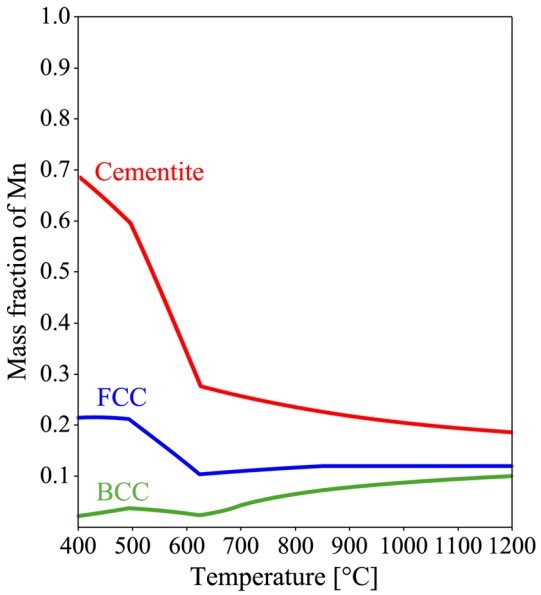

Fig. 8 Distribution of manganese among the phases cementite, FCC = austenite, and BCC = ferrite

manganese in cementite, ferrite, and austenite as a function of temperature, as shown in Fig. 8. As can be seen, the cementite carbide is strongly enriched by manganese below 625 °C. This result indicates that for the Fe–12Mn–1C composition the partitioning of manganese occurs at 625 °C. Thus, a growth mechanism controlled by manganese is expected to occur at the 600 °C reaction temperature presented in this work.

Conclusion

The TTT-diagram corresponding to pearlite formation in Fe–12Mn–1C Hadfield steel was built by means of isothermal reactions. The obtained results show that pearlite formation is relatively fast in this alloy in contrast to the Fe–12Mn–0.8C composition mostly found in literature. In this regard, the increase in carbon content from 0.8 to 1 wt.% accelerates the reaction by a factor of 6. While in the 0.8 wt.% carbon alloy the reaction starts after 40 min at 550 °C, only 7 min is needed in the 1 wt.% carbon alloy at the same temperature. Pearlite formation is initiated on the grain boundaries, and intergranular colonies evolve with reaction time. The Fe–12Mn–1C Hadfield steel seems to reach a saturation value of 35% pearlite fraction after 150 min at 550 °C. Accordingly, pearlite formation can occur during alloy production, or post-processing operations, if quenching, or cooling operations, are not severe enough.

Acknowledgments The authors acknowledge the support of CONICET, Argentina, under Grants PIP 0488 and PDTS-251.

References

1. M. Martín, M. Raposo, A. Druker, C. Sobrero, J. Malarría, Influence of Pearlite Formation on the Ductility Response of Commercial Hadfield Steel. Metallogr. Microstruct. Anal. **5**, 505 (2016)
2. Y. Ono, T. Tsuchiyama, and S. Takaki, Mechanism of Embrittlement in Hadfield Steel, in *Steels and Materials for Power Plants* (Wiley, New York, 2006) FRG, pp. 143–148
3. S.A. Hackney, G.J. Shiflet, The Pearlite-Austenite Growth Interface in an Fe–0.8 C–12 Mn alloy. Acta Met. **35**, 1007 (1987)
4. S.A. Hackney, G.J. Shiflet, Pearlite Growth Mechanism. Acta Met. **35**, 1019 (1987)
5. S.A. Hackney, Morphological Instabilities and Branching Processes at the Initiation of the Eutectoid Transformation. Scr. Metall. Mater. **25**, 1453 (1991)
6. S.A. Hackney, G.J. Shiflet, Interfacial Structure at the pearlite: Austenite Growth Interface in an Fe–0.8C–12Mn Steel. Scr. Metall. **19**, 757 (1985)
7. R.J. Dippenaar, R.W.K. Honeycombe, The Crystallography and Nucleation of Pearlite. Proc. R. Soc. A Math. Phys. Eng. Sci. **333**, 455 (1973)
8. D.S. Zhou, G.J. Shiflet, Ferrite: Cementite Crystallography in Pearlite. Met. Trans. A **23**, 1259 (1992)
9. C.R. Hutchinson, G.J. Shiflet, The Formation of Partitioned Pearlite at Temperatures Above the Upper Ae1 in an Fe–C–Mn Steel. Scr. Mater. **50**, 1 (2004)
10. A.Y.M. Ontman, G.J. Shiflet, Thermodynamic Mapping of Austenite Decomposition's Approach Toward Equilibrium in Fe–C–Mn at 700 °C. Acta Mater. **89**, 98 (2015)
11. M.X. Zhang, P.M. Kelly, The Morphology and Formation Mechanism of Pearlite in Steels. Mater. Charact. **60**, 545 (2009)
12. R.F. Mehl, W.C. Hagel, The Austenite: Pearlite Reaction. Prog. Met. Phys. **6**, 74 (1956)
13. N. Zhong, X. Wang, Z. Guo, Y. Rong, Orientation Relationships between Ferrite and Cementite by Edge-to-edge Matching Principle. J. Mater. Sci. Technol. **27**, 475 (2011)
14. Y. Ono, T. Tsuchiyama, S. Takaki, Microstructural Change during Isothermal Aging in High Manganese Austenitic Steels. Tetsu-to-Hagane **84**, 309 (1998)
15. D.A. Porter, K.E. Easterling, *Phase Transformations in Metals and Alloys* (Chapman and Hall, London, 1992), p. 333
16. C. Scott, S. Allain, M. Faral, N. Guelton, The Development of a New Fe–Mn–C Austenitic Steel for Automotive Applications. Rev. Métallurgie **103**, 293 (2006)
17. N. Ridley, The Pearlite Reaction, in *Proceedings of International Conference on Phase Transformations in Ferrous alloys*, eds. by A.R. Marder, J.I. Goldstein (TMS-AIME, Warrendale, 1984), p. 201–236
18. M. Hillert, Analysis of the Effect of Alloying Elements on the Pearlite Reaction, in *Proceedings of an International Conference on Solid to Solid Phase Transformations*, ed. by H.I. Aaronson (TMS-AIME, Warrendale, 1982), p. 789–806
19. H.K.D.H. Bhadeshia, D.V. Edmonds, The Bainite Transformation in a Silicon Steel. Metall. Trans. A **10**, 895 (1979)
20. B.C. De Cooman, Structure-Properties Relationship in TRIP Steels Containing Carbide-Free Bainite. Curr. Opin. Solid State Mater. Sci. **8**, 285 (2004)
21. H. Dierkes, R. Dronskowski, High-Resolution Powder Neutron Diffraction on Mn3C. Zeitschrift Fur Anorg. Und Allg. Chemie **640**, 3148 (2014)
22. J.D. Verhoeven, *Fundamentals of Physical Metallurgy* (Wiley, New York, 1975), p. 458
23. C.R. Hutchinson, R.E. Hackenberg, G.J. Shiflet, The Growth of Partitioned Pearlite in Fe–C–Mn Steels. Acta Mater. **52**, 3565 (2004)
24. N.A. Razik, G.W. Lorimer, N. Ridley, An Investigation of Manganese Partitioning During the Austenite–Pearlite Transformation Using Analytical Electron Microscopy. Acta Met. **22**, 1249 (1974)